

# Conformational Analysis of Lipophilic Antifolates: Crystal Structure of 2-Amino-4-oxo-6-adamantylpteridine and a Comparison of Its Binding to Bacterial and Avian Dihydrofolate Reductase

Mary McCourt and Vivian Cody\*

Contribution from the Medical Foundation of Buffalo, 73 High Street, Buffalo, New York 14203.  
Received August 17, 1990

**Abstract:** The crystal structure of 2-amino-4-oxo-6-adamantylpteridine (DOPT), a folate analogue of the potent lipophilic antifolate, 2,4-diamino-6-adamantylpteridine (DAPT), which is selective for mammalian dihydrofolate reductase (DHFR), was determined to examine its conformational features and to define its mode of binding to the enzyme DHFR. DOPT crystallized as an ethanesulfonate salt in the monoclinic space group  $P2_1/c$  with cell dimensions  $a = 20.261$  (7) Å,  $b = 16.357$  (2) Å,  $c = 12.317$  (3) Å,  $\beta = 93.76$  (2)°, and  $Z = 8$ . The pteridine ring is protonated at N(1) to form the ethanesulfonate salt. A theoretical study of the binding characteristics of the folate, DOPT, the antifolate model, DAPT, and the pyrimidine analogue, 2,4-diamino-5-adamantyl-6-methylpyrimidine, DAMP, to both chicken and *Lactobacillus casei* DHFR was carried out with YEP1, a molecular mechanics program which optimized the DHFR-inhibitor interactions. The objective of these calculations was to determine characteristics of binding that would aid in explaining the species specificity and selectivity of DAMP and DAPT. These studies indicate that there is a correlation between the size of a specific enzyme active site and antifolate activity, i.e., the antifolates DAPT and DAMP have more unfavorable intermolecular interactions in the bacterial enzyme than in chicken liver DHFR, consistent with their biological activity. These studies further indicate that DOPT, the oxidized analogue of DAPT, is not likely to bind in the folate orientation.

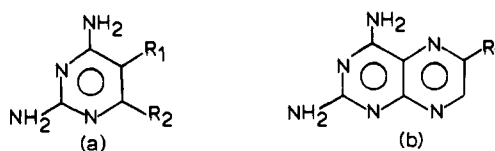
## Introduction

The enzyme dihydrofolate reductase (DHFR), present in all cells, is a necessary component for cell growth and is responsible for maintaining intracellular folate pools in their biochemically active reduced state. The enzyme can also be strongly and specifically inhibited by certain substrate analogues with binding affinities so great that they are not readily displaced by the natural folic acid substrates. The effect of this inhibition is to deplete intracellular reduced folates required for one carbon transfer reactions and interfere with de novo thymidine and purine synthesis. Because of this important metabolic role, inhibition of DHFR by potent antifolates has been the focus of chemotherapy of infectious and neoplastic disease.<sup>1,2</sup> Some of the most recent uses of antifolates have been in the treatment of the opportunistic infections that occur in AIDS patients.<sup>3,4</sup>

Structure activity data on a series of lipophilic pyrimidine and pteridine antifolates revealed that an adamantyl group in the 5-position of pyrimidine antifolates such as 2,4-diamino-5-adamantyl-6-methylpyrimidine (DAMP) produces the most effective inhibitors of mammalian DHFR with potencies greater than methotrexate (MTX)<sup>5</sup> (Table I). These data also indicated that adamantylpteridines, such as 2,4-diamino-6-adamantylpteridine (DAPT), while not as potent as their pyrimidine analogues, were still selective mammalian DHFR inhibitors.<sup>6</sup> DAMP, which was subsequently tested in phase I clinical trials,<sup>7</sup> and DAPT, were inactive in the bacterial enzyme assay.

Crystallographic data delineating the DHFR enzyme structure and inhibitor complexes are available from bacterial, avian, mouse, and human sources<sup>8-14</sup> and show that the active site is located

**Table I.** Structure Activity Relationships of Lipophilic Inhibitors of DHFR



	6-R2	name	mammalian <sup>5</sup> (m)	bacterial <sup>6</sup> (m)
		(a) 5-R1		
adamantyl	propyl	DAPP	$4.8 \times 10^{-8}$	
adamantyl	ethyl	DAEP	$2.5 \times 10^{-10}$	
adamantyl	methyl	DAMP	$6.0 \times 10^{-9}$	$>10^{-5}$
adamantyl	hydrogen	DAHP	$3.3 \times 10^{-7}$	
		(b) 6-R1		
<i>p</i> -amino-benzoyl-glutamate		MTX	$8.8 \times 10^{-8}$	
adamantyl		DAPT	$1.4 \times 10^{-7}$	$>10^{-5}$

within an L-shaped cavity cutting across one face of the enzyme. The antifolate pterine moiety binds within the cavity, which forms an ionic interaction with the acidic residue and is perpendicular to the *p*-aminobenzoylglutamate moiety which extends to the protein surface. These structural data also reveal that antifolates such as MTX are protonated at N(1) and form N(1)/N(2) ionic interactions with Asp-26 in *L. casei* and Glu-30 in chicken liver DHFR. More recent structural data on human DHFR-folate complexes<sup>14</sup> revealed that folates bind in a different orientation

(1) Blakely, R. L. *Folates and Pteridines*; Blakeley, R. L., Benkovic, S. J., Eds.; John Wiley & Sons: New York, 1984; Vol. 1, pp 191-253.

(2) Roth, B. *Handbook of Experimental Pharmacology*; Hitchings, G. H., Ed.; Springer-Verlag: New York, 1983; Vol. 64, pp 107-127.

(3) Araujo, F. G.; Guptill, D. R.; Remington, J. S. *J. Infect. Dis.* **1987**, *156*, 828.

(4) Queener, S. F.; Bartlett, M. S.; Jay, M. A.; Durkin, M. M.; Smith, J. W. *Antimicrob. Agents Chemother.* **1987**, *31*, 1323.

(5) Jonak, J. P.; Zakrzewski, S. F.; Mead, L. H. *J. Med. Chem.* **1971**, *14*, 408.

(6) Jonak, J. P.; Zakrzewski, S. F.; Mead, L. H.; Allhouse, L. D. *J. Med. Chem.* **1972**, *15*, 1331.

(7) Cody, V.; Zakrzewski, S. F. *J. Med. Chem.* **1982**, *25*, 427.

(8) Bolin, J. T.; Filman, D. J.; Matthews, D. A.; Hamlin, R. C.; Kraut, J. *J. Biol. Chem.* **1982**, *257*, 13650.

(9) Matthews, D. A.; Bolin, J. T.; Burridge, J. M.; Filman, D. J.; Volz, K. W.; Kaufman, B. T.; Beddell, C. R.; Champness, J. N.; Stammers, D. K.; Kraut, J. *J. Biol. Chem.* **1985**, *260*, 392.

(10) Stammers, D. K.; Champness, J. N.; Beddell, C. R.; Dann, J. G.; Eliopoulos, E.; Geddes, A. J.; Ogg, D.; North, A. C. T. *FEBS Lett.* **1987**, *218*, 178.

(11) Oefner, C.; D'Arcy, A.; Winkler, F. K. *Eur. J. Biochem.* **1988**, *174*, 377.

(12) Kraut, J.; Matthews, D. A. *Biological Macromolecules and Assemblies*; Jurnak, F., McPherson, A., Eds.; John Wiley & Sons: New York, 1987; Vol. 111, pp 1-71.

(13) Bystroff, C.; Oatley, S. J.; Kraut, J. *Biochemistry* **1990**, *29*, 3263.

(14) Davis, J. A.; Delcamp, T. S.; Prendergrast, N. J.; Asford, V. A.; Freisheim, J. H.; Kraut, J. *Biochemistry* **1990**, *29*, 9467.

such that N(2) and N(3) form the ionic interactions with the Glu-30 oxygens. Moreover, structural data have also shown that DAMP occupies the pterine portion of the active site in the same manner as MTX.<sup>9</sup>

Numerous computational efforts have been carried out to study the interactions of DHFR inhibitors with the goal of rational drug design.<sup>15-19</sup> These studies revealed that new antifolates could be designed with improved binding affinities<sup>15,16</sup> and that when the enzyme structure was allowed complete flexibility in molecular dynamics<sup>17</sup> and free energy perturbation<sup>18</sup> simulations, the enzyme backbone maintained a conformation similar to that of its crystallographically observed starting structure.

As part of a program to determine the structural properties of antifolates and their binding interactions in DHFR, we report the crystal structure of 2-amino-4-oxo-6-adamantylpteridine (DOPT) as well as the theoretically modeled binding interactions of DOPT, DAPT, and DAMP (Figure 1) with both *Lactobacillus casei* and chicken liver DHFR. These theoretical calculations extend previous studies<sup>19</sup> with the program YETI<sup>20</sup> which incorporates a hydrogen-bonding function into its energy term that is based on hydrogen bond characteristics of small-molecule molecular packing. YETI results provide structural and energetic information that suggest reasons for species specificity and selectivity as well as a prediction as to whether DOPT would likely bind as a folate. The calculations also provide an insight into the impact of folate versus antifolate binding for a rigid inhibitor.

### Experimental Section

**X-ray Structure Determination.** Crystals of DOPT were grown from solutions containing ethanesulfonic acid (ES). Crystal data showed the following: space group  $P2_1/c$ , monoclinic,  $a = 20.261(7) \text{ \AA}$ ,  $b = 16.357(2) \text{ \AA}$ ,  $c = 12.317(3) \text{ \AA}$ ,  $\beta = 93.76(2)^\circ$ ,  $V = 4073.16 \text{ \AA}^3$ ,  $Z = 8$ ,  $D_{\text{calc}} = 1.326 \text{ g cm}^{-3}$ . The crystal used for data collection was rectangular with dimensions  $0.40 \times 0.40 \times 0.60 \text{ mm}$ . Data were collected on a Siemens P3 diffractometer with Mo  $K\alpha$  ( $0.7107 \text{ \AA}$ ) radiation. The crystal was stable and showed no deterioration during data collection. The X-ray diffraction data were corrected for Lorentz and polarization effects but not for extinction or absorption effects. A total of 11942 unique reflections were collected to  $\theta = 60^\circ$  with  $8262 I > 2\sigma(I)$ . The structure was solved by using the direct methods program SHELX84.<sup>21</sup> Non-hydrogen atom thermal parameters were made anisotropic and refined by full-matrix least-squares techniques. Hydrogen atoms were located in Fourier difference maps and given isotropic thermal parameters one unit greater than the heavy atoms to which they were bound; their thermal parameters were held constant during refinement. The final  $R$  index was 0.083 for 4891 data with  $I > 4\sigma(I)$  and  $\sin(\theta/\lambda) = 0.60$ . During the course of refinement it became evident that the antifolate had become oxidized to the 4-oxofolate of the starting material and that the ethyl side chain of one of the ethanesulfonate molecules was rotationally disordered with 60/40% occupancy for C(22A) and C(22B), respectively.

**Molecular Modeling.** DAPT, the antifolate analogue of DOPT, was built based on the crystal structure of DOPT by replacing the 4-oxo with an  $\text{NH}_2$  group (Figure 1b). The starting antifolate models for *L. casei* DHFR were based on the ternary crystal structure of the MTX-NADPH complex<sup>9</sup> in which the 2,4-diaminopyrimidine moiety of DAMP and DAPT were fit to that of MTX. This ensured that the model included the protonation of N(1) and the hydrogen bonding of N(2) of the antifolate by Asp-26 of *L. casei*. The antifolate models for chicken liver DHFR were designed by modeling the inhibitors into the active site, monitoring the distance between the oxygens of Glu-30 and N(1), N(2), and defining a directionality by maintaining coplanarity between the Glu-30 oxygens and N(1), N(2). The folate models for both *L. casei* and chicken liver DHFR were made by least-squares fitting the folate N(1),

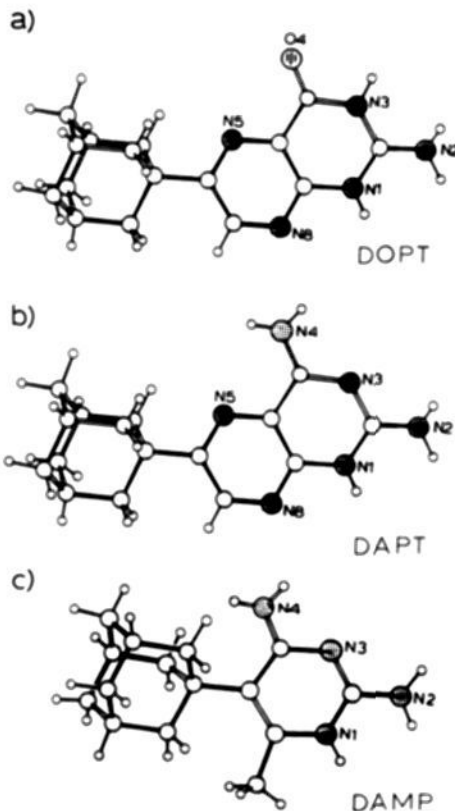


**Figure 1.** Molecular conformation of (a) 2-amino-4-oxo-6-adamantylpteridine (DOPT), (b) a model of 2,4-diamino-6-adamantylpteridine (DAPT), and (c) 2,4-diamino-5-adamantyl-6-methylpyrimidine (DAMP).

N(2), and N(3) atomic positions to the N(3), N(2), and N(1) antifolate atomic positions, respectively.

**Molecular Mechanics.** The recently developed YETI program<sup>20</sup> is a molecular mechanics minimization method that uses a fixed backbone and allows the side chains to move. YETI as a methodology lies somewhere between simple graphics modeling and a full molecular mechanics program, such as AMBER<sup>22</sup> or CHARM, in which the entire protein is allowed conformational flexibility. YETI is also the only program that incorporates a directed hydrogen bond term parameterized based on structural information as well as a metal center term.

Inhibitor-enzyme interactions were evaluated on the basis of electronic, van der Waals, and hydrogen-bonding interactions by using the program YETI running on a VAX 8600. Translational and rotational degrees of freedom were permitted for the inhibitor and cofactor. The protein was restricted to conformational flexibility of its side chains, and NADPH was allowed no torsional flexibility. Connectivity for the protein is based on a residue library, and inhibitor and cofactor connectivity is defined by the user in a topology file. YETI places hydrogen atoms ( $1.0 \text{ \AA}$ ) on all polar atoms and assigns partial charges to the amino acids and water molecules. Atomic partial charges for the inhibitors DAMP and DAPT as well as the folate DOPT and the cofactor NADPH were determined with the MNDO program found in the AMPAC package on the SYBYL system.<sup>24</sup> YETI analyzes all pairs of interactions, nonbonded and bonded.

For the present calculations a zone refinement was used in which the inhibitor was chosen as the center of a  $20.0\text{-\AA}$  sphere. The minimization routine relaxes all residues in the zone, including amino acid side chains, inhibitor, cofactor, and the waters that are a part of the crystal structure. A distance-dependent dielectric of  $2(R)$  was used consistent with the program parameterization. As the optimization proceeds, the program checks both the change in energy as well as the RMS derivatives (torsion, global rotation, and global translation) for each cycle. In these calculations convergence was achieved when the change in energy between the cycles was less than  $0.500 \text{ kcal/mol}$  and the RMS derivatives dropped below  $0.250^\circ$ ,  $0.500^\circ$ , and  $5.00 \text{ \AA}$ , respectively. The convergence routine changes from steepest descent to conjugate gradient after the first 20 cycles of refinement.

(15) Kuyper, L. *Computer Aided Drug Design, Methods and Applications*; Perun, T., Propst, C., Eds.; Marcel Dekker, Inc.: New York, 1989; pp 327-369.

(16) Blaney, J. M.; Hansch, C.; Silipo, C.; Vittoria, A. *Chem. Rev.* **1984**, *84*, 333.

(17) Bauber-Osguthorpe, P.; Roberts, V. A.; Osguthorpe, D. J.; Wolff, J.; Genest, M.; Hagler, A. T. *Proteins: Struct. Funct. Genet.* **1988**, *4*, 31.

(18) Fleischmann, S. H.; Brooks III, C. L. *Proteins: Struct. Funct. Genet.* **1990**, *7*, 52. Brooks III, C. L.; Fleischman, S. H. *J. Am. Chem. Soc.* **1990**, *112*, 3307.

(19) Sutton, P. A.; Cojy, V. *J. Am. Chem. Soc.* **1988**, *110*, 6219.

(20) Vedani, A.; Huhta, D. W. *J. Am. Chem. Soc.* **1990**, *112*, 4759.

(21) Sheldrick, G. SHELX84. *Program for Crystal Structure Solution*; University of Gottingen, Republic Federal of Germany, 1984.

(22) Kollman, P. *Acc. Chem. Res.* **1985**, *18*, 105.

(23) Brooks, B. R. et al. CHARM, *J. Comput. Chem.* **1983**, *4*, 187.

(24) SYBYL; Tripos Associates, St. Louis, MO 63117.

**Table II.** Atomic Coordinates ( $\times 10^4$ ) and Isotropic Equivalent Thermal Parameters ( $\times 10^3$ ) for 2-Amino-4-oxo-6-adamantylpteridine Ethanesulfonate Salt<sup>a</sup>

atom	X/A ( $\sigma$ )	Y/B ( $\sigma$ )	Z/C ( $\sigma$ )	$B_{iso}$ ( $\sigma$ )
C(2)	8275 (2)	3499 (3)	2073 (4)	37 (1)
C(4)	9479 (2)	3566 (3)	2249 (4)	41 (1)
C(4A)	9428 (2)	3525 (3)	3444 (4)	36 (1)
C(6)	9908 (2)	3522 (2)	5163 (4)	38 (1)
C(8A)	8808 (2)	3493 (3)	3857 (4)	37 (1)
C(9)	10541 (2)	3538 (2)	5888 (4)	38 (1)
C(10)	10943 (3)	4314 (3)	5622 (5)	48 (1)
C(11)	11596 (3)	4315 (4)	6325 (6)	55 (2)
C(12)	11460 (3)	4337 (4)	7520 (6)	62 (2)
C(13)	11069 (3)	3551 (4)	7797 (5)	52 (2)
C(14)	10416 (3)	3547 (3)	7099 (4)	44 (1)
C(15)	10962 (3)	2784 (3)	5645 (5)	45 (1)
C(16)	11618 (3)	2797 (4)	6349 (5)	52 (2)
C(17)	12004 (3)	3557 (4)	6091 (6)	60 (2)
C(18)	11471 (3)	2802 (4)	7549 (6)	59 (2)
N(1)	8242 (2)	3496 (3)	3152 (3)	40 (1)
N(2)	7740 (2)	3513 (3)	1435 (3)	52 (1)
N(3)	8879 (2)	3504 (3)	1655 (3)	42 (1)
N(5)	9977 (2)	3541 (3)	4089 (3)	40 (1)
N(8)	8722 (2)	3491 (3)	4913 (3)	41 (1)
O(4)	9985 (2)	3653 (3)	1798 (3)	62 (1)
C(2')	6703 (2)	1524 (3)	1956 (4)	40 (1)
C(4')	5498 (2)	1425 (3)	1898 (4)	43 (1)
C(4A')	5559 (2)	1488 (2)	3106 (4)	38 (1)
C(6')	5080 (2)	1491 (3)	4727 (4)	39 (1)
C(7')	5720 (2)	1561 (3)	5242 (4)	42 (1)
C(8A')	6179 (2)	1543 (3)	3638 (4)	37 (1)
C(9')	4461 (2)	1436 (3)	5340 (4)	41 (1)
C(10')	4595 (3)	1490 (4)	6579 (4)	47 (1)
C(11')	3942 (3)	1452 (4)	7150 (5)	57 (2)
C(12')	3597 (3)	643 (5)	6868 (6)	64 (2)
C(13')	3455 (3)	593 (4)	5667 (7)	63 (2)
C(14')	4107 (3)	630 (4)	5065 (5)	52 (2)
C(15')	4000 (3)	2158 (3)	4972 (4)	46 (1)
C(16')	3351 (3)	2103 (4)	5543 (5)	53 (2)
C(17')	3500 (3)	2165 (4)	6762 (5)	57 (2)
C(18')	3009 (3)	1302 (5)	5246 (6)	65 (2)
N(2')	7238 (2)	1529 (3)	1430 (3)	49 (1)
N(5')	5005 (2)	1454 (3)	3647 (3)	41 (1)
N(8')	6270 (2)	1583 (3)	4707 (3)	42 (1)
O(4')	4992 (2)	1352 (3)	1357 (3)	64 (1)
C(21)	8819 (4)	194 (5)	3480 (6)	68 (2)
C(22A)	8892 (1)	-249 (11)	4537 (15)	100 (6)
C(22B)	8452 (12)	-273 (13)	2666 (24)	94 (8)
O(1)	7908 (2)	1139 (3)	4194 (3)	53 (1)
O(2)	9041 (2)	1575 (3)	4439 (3)	54 (1)
O(3)	8477 (2)	1611 (3)	2653 (3)	51 (1)
S(1)	8546 (1)	1210 (1)	3705 (1)	40 (1)
C(21')	6309 (4)	4917 (6)	3454 (7)	80 (3)
C(22')	6318 (5)	5331 (5)	4543 (10)	95 (3)
O(1')	7115 (2)	3790 (3)	4169 (3)	50 (1)
O(2')	5954 (2)	3495 (3)	4146 (3)	54 (1)
O(3')	6505 (2)	3532 (4)	2476 (3)	71 (2)
S(2)	6469 (1)	3854 (1)	3564 (1)	45 (1)

<sup>a</sup>  $B_{iso} = \frac{8}{3} \pi^2 \sum_i \sum_j U_{ij} a_i^* a_j^* a_{ij}$ . The second set of independent DOPT ES molecules are labeled with primes.

## Results

**Crystal and Molecular Structure Analysis.** Heavy atom positions of DOPT ES salt are listed in Table II, and the molecular conformation of DOPT is shown in Figure 1a. The conformation of each of the two independent DOPT molecules is planar, and each has nearly identical geometries and conformations. Because of the equivalent environment of the adamantyl ring, rotation about the pteridine-adamantyl bond results in conformationally equivalent rotamers every 120°. The torsion angles involving the tertiary carbon C(9) [C(7)-C(6)-C(9)-C(10); C(14) and C(15), respectively] are 0 and  $\pm 120^\circ$ , similar to that observed in other pyrimidine adamantyl antifolates.<sup>25</sup>

(25) Cody, V.; Sutton, P. A.; Welsh, W. J. *J. Am. Chem. Soc.* **1987**, *109*, 4053.

**Table III.** Hydrogen Bond Contacts in DOPT ES

D-H...A	D-H (Å)	H...A (Å)	D...A (Å)	<D-H...A (deg)
N(1)H...O(1')	0.83	1.92	2.72	161
N(2)HA...O(3')	0.95	1.93	2.88	174
N(2)HB...O(1)	0.73	2.17	2.87	161
N(3)H...O(2)	0.88	1.91	2.78	173
N(1')H...O(1)	0.96	1.81	2.76	170
N(2')HA...O(3)			2.83	
N(2')HB...O(1')	0.72	2.11	2.83	176
N(3')H...O(2')	0.79	2.02	2.81	175

Generally, the bond lengths and angles of pyrimidine, pteridine, and quinazoline antifolates reflect their protonation state.<sup>19,25-27</sup> The differences between protonated and nonprotonated antifolates are manifested by shortening of the exocyclic amino bonds and lengthening of the adjacent pyrimidine moiety endocyclic C-N bonds, in addition to large angular changes at the N(1), C(2), and C(8a) positions. The average geometry at C(2) [i.e., C(2)-N(1) (1.338); C(2)-N(3) (1.350); C(2)-N(2) (1.298)] is indicative of protonation at N(1) of DOPT. The difference between the C(2)-N(2) and C(4)-O(4) bond lengths (1.298 vs 1.199 Å, respectively), when compared to that in MTX<sup>26</sup> (1.281 and 1.305 Å, respectively), is indicative that the 4-substituent has been oxidized to an oxygen. The resonance structure of the pteridine ring at the N(3)-C(4) and C(8a)-N(1) bonds further reflects a 4-oxo influence as observed in other folylpteridine structures.<sup>28,29</sup>

As demonstrated by the data in Table III, the hydrogen bonding involving the pteridine nitrogen atoms reveals a pattern of N(1) protonation by an acidic oxygen of ES and hydrogen bond donation by N(2) to an adjacent oxygen, remarkably similar to that observed for MTX in the enzyme-bound structure.<sup>8,9</sup> An equivalent arrangement is made with N(3) and N(2) to the second ES in the structure. This symmetrical hydrogen bonding involving two sulfate oxygen atoms of a single ES is not observed in the structure of the DAMP ES salt.<sup>7</sup> There are no interactions involving O(4) of DOPT, and the molecular packing shows the DOPT ES molecules form alternating layers of hydrophobic and hydrophilic surfaces.

**Molecular Modeling.** Modeling studies with *L. casei* and chicken liver DHFR were performed on an active-site region comprising those residues within a 20 Å sphere from the center of the inhibitor. In the case of the bacterial enzyme this included 162 residues, 2 water molecules, and the cofactor NADPH as well as DAMP, DAPT, and DOPT in a series of three separate calculations. In the chicken liver enzyme it included 186 residues, 2 water molecules, and NADPH as well as DAMP, DAPT, and DOPT, respectively.

**DHFR Models.** The starting antifolate and folate models in all instances showed that several residues make close (H...H or H...X) intermolecular contacts involving the adamantyl group, which are less than the sum of their van der Waals radii. However, as illustrated (Figure 2), the effect of the antifolate DAPT versus folate DOPT binding places the adamantyl group in different regions of the active site. The net result is that the short contacts are to different regions of the adamantyl group.

**DAMP.** As shown in Table IV, when DAMP was modeled in the antifolate mode in bacterial DHFR, the closest intermolecular contacts involved Leu-4, Phe-30, and Phe-49. To relieve these close contacts, the optimization procedure moves the adamantyl group toward Phe-30 which simultaneously swings aside (Figure 3). Similar movements take place with Phe-49 and Leu-4. There is a reorientation of the starting hydrogen bonds to Asp-26. In addition, there is little movement of the cofactor, NADPH, in spite of several short contacts to DAMP.

(26) Sutton, P. A.; Cody, V.; Smith, G. D. *J. Am. Chem. Soc.* **1986**, *108*, 4155.

(27) Sutton, P. A.; Cody, V. *J. Med. Chem.* **1987**, *30*, 1843.

(28) Mastropaolo, D.; Camerman, A.; Camerman, N. *Science* **1980**, *210*, 334.

(29) Fontecilla-Camps, J. C.; Bugg, C. E.; Temple, C., Jr.; Rose, J. D.; Montgomery, J. A.; Kisliuk, R. L. *J. Am. Chem. Soc.* **1979**, *101*, 6114.

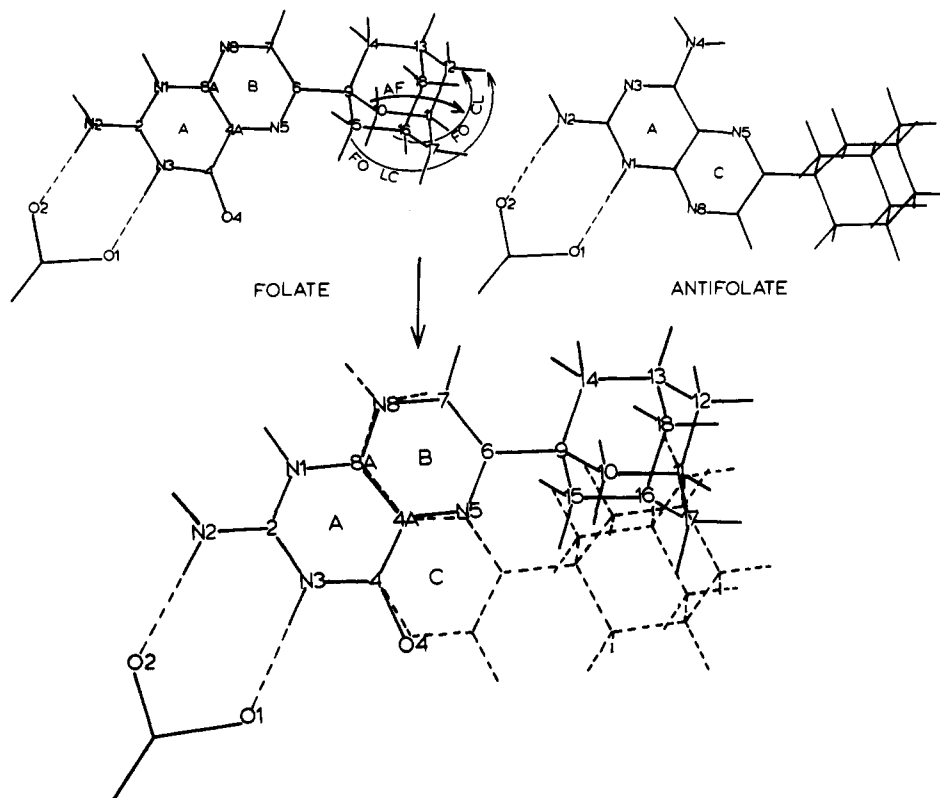


**Figure 2.** Model showing the superposition of DAPT (dashed line) in an antifolate (AF) orientation and DOPT (solid line) in the folate (FO) orientation. The antifolate model is rotated  $180^\circ$  along the N(2)-C(9) direction, with N(2) fixed, to obtain the folate orientation. Note that in both models N(2) and N(1)/N(3) form hydrogen bonds to the enzyme acidic function. Also illustrated are the close contact regions of the adamantyl ring with both the bacterial (Lc) and avian (cl) enzyme.

**Table IV.** Shortest Contacts (Å) of DAMP, DAPT, and DOPT in the Active Site of *L. casei* DHFR Before and After YET<sub>1</sub> Minimization

antifolate orientation							folate orientation			
residue	DAMP enz-inhib	start	after	DAPT enz-inhib	start	after	residue	DOPT enz-inhib	start	after
NADPH	(C4-H15)	1.91	2.16	(C5-H10)	1.91	2.98	NADPH	(C5-H15)	1.22	4.34
Leu-4	(O-HN4)	1.69	1.87	(O-HN4)	1.70	1.94	Leu-4	(C-HN1)	2.72	3.57
Asp-26	(OD1-HN1)	1.93	1.83	(OD1-HN1)	1.62	1.83	Asp-26	(OD1-H3)	1.64	2.53
Phe-30	(CZ-H16)	1.25	2.33				Val-41	(CE1-H12)	2.77	4.20
Thr-45	(CG2-H16)	2.15	2.46	(CG2-H17)	0.78	2.29	Thr-45	(CG2-C13)	0.66	3.34
Ser-48	(HOG-H10)	3.63	4.07	(HOG-H17)	0.67	1.89	Ser-48	(HOG-H17)	1.56	3.30
Phe-49	(CE1-H12)	1.27	2.30	(CE1-H16)	1.18	2.39	Phe-49	(CE1-H11)	1.53	2.50

**Table V.** Shortest Contacts (Å) of DAMP, DAPT, and DOPT in the Active Site of Chicken Liver DHFR Before and After YET<sub>1</sub> Minimization

antifolate orientation						folate orientation				
residue	DAMP enz-inhib	start	after	DAPT enz-inhib	start	after	residue	DOPT enz-inhib	start	after
NADPH	(C4-HN4)	3.16	2.93	(O2'-H11)	2.56	3.70	NADPH	(O-H16)	2.41	>4.5
Leu-22	(CD1-H61)	2.71	2.74	(CD1-H7)	2.50	3.11	Asn-21	(OD1-H17)	2.84	4.02
Glu-30	(OE1-HN2)	2.11	1.92	(OE1-H2B)	1.89	1.89	Glu-30	(OE1-H2A)	1.86	1.93
Phe-34	(CE2-H14)	2.60	2.44	(CE1-HN4)	2.98	3.76	Phe-34	(CD1-HN1)	2.74	3.47
Ile-60	(CE1-H12)	2.61	2.99	(N-H17)	2.49	3.77	Ser-59	(OG-H18)	0.24	2.74
							Ile-60	(CG1-H12)	1.30	2.51

The original starting model of DAMP in chicken DHFR has few short contacts to the surrounding residues. The model starts with two well-defined hydrogen bonds as determined by YET<sub>1</sub> which are maintained during minimization. DAMP moves up relative to its original starting position, in a manner similar to that in the bacterial enzyme.

**DAPT.** When DAPT was modeled into the antifolate MTX site of *L. casei*, the closest contacts involve Thr-45, Ser-48, and Phe-49 (Table IV). YET<sub>1</sub> optimization causes DAPT to tilt away from the cofactor in order to relieve these extremely short contacts by the simultaneous swing of Phe-30, Ser-48, and Phe-49 away from the inhibitor. There is a realignment of the hydrogen bonds of N(1) and N(2) to Asp-26. The movement of NADPH is similar to that observed in the DAMP antifolate optimization.

For the model of DAPT in chicken DHFR, the closest contacts are to Asn-21, Glu-30, and Ile-60 (Table V). Refinement causes

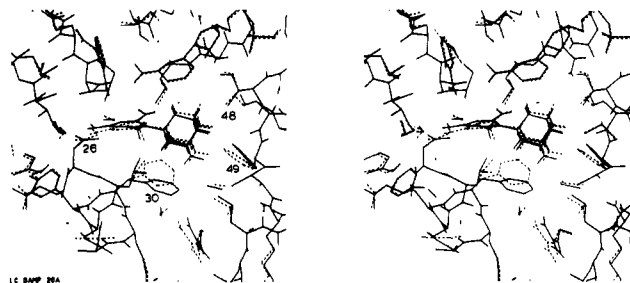


**Figure 3.** Stereo comparison of the YET<sub>1</sub> optimization of DAMP in *L. casei* DHFR. Dashed line is starting model, solid line after minimization.

DAPT to pivot down around N(2) and twist which results in its moving further into the active site cavity (Figure 4). Phe-34

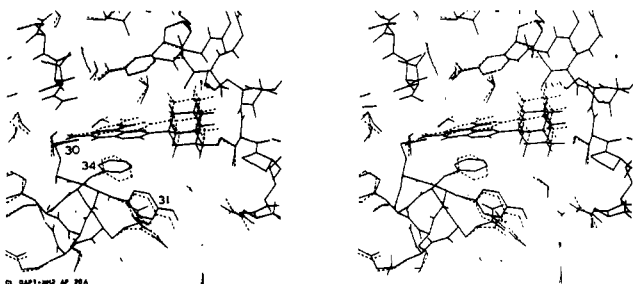


**Figure 4.** Stereo comparison of the YETI optimization of DAPT in chicken liver DHFR. Dashed line is starting model, solid line after minimization.

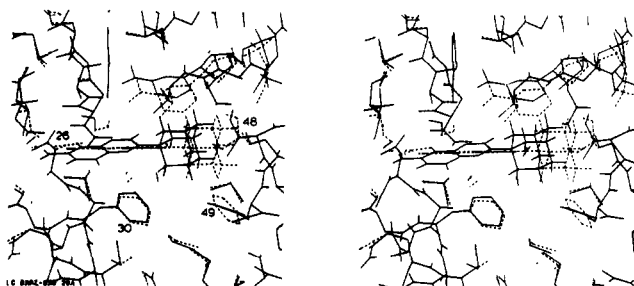


**Figure 5.** Stereo comparison of the YETI optimization of DOPT in *L. casei* DHFR. Dashed line is starting model, solid line after minimization.

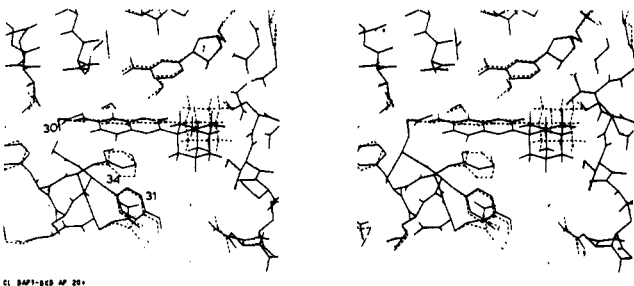


**Figure 6.** Stereo comparison of the YETI optimization of DOPT in chicken liver DHFR. Dashed line is starting model, solid line after minimization.

swings away from DAPT, and there is a slight movement of NADPH. Glu-30 twists away from the DAPT and moves further into the active site cavity, while maintaining good hydrogen bonds as defined by YETI to the N(1) and N(2) atoms of DAPT.

**DOPT.** The shortest starting contacts for the folate DOPT to its surrounding residues in bacterial DHFR involves Thr-45, Ser-48, Phe-49, and Ala-97 (Table IV). Optimization causes DOPT to move further into the active site cavity and alter the hydrogen-bonding pattern to Asp-26 with large movements in the Asp-26 side chain in concert with that of Thr-116 (Figure 5). The shortest contacts are relieved through the movement of NADPH as well as the twisting of Phe-30, Ser-48, and Phe-49.

The closest contacts of the surrounding residues in chicken DHFR to DOPT in the starting model are to Thr-56, Ser-59, and Ile-60. DOPT moves by twisting down relative to its starting position and moving further into the active site. There is a twisting of the Glu-30 oxygens causing them to also move further into the active site. NADPH moves down in the same direction as does the DOPT with Phe-34 and Tyr-31 twisting away from the DOPT molecule (Figure 6).

### Discussion

Activity data show that both DAMP and DAPT are active in mammalian DHFR enzymes but are inactive in bacterial DHFR. In an effort to understand this species specificity and selectivity, the techniques of modeling and molecular mechanics energy calculations were used to study the interactions of DAMP and DAPT in the active sites of *L. casei* and chicken liver DHFR in

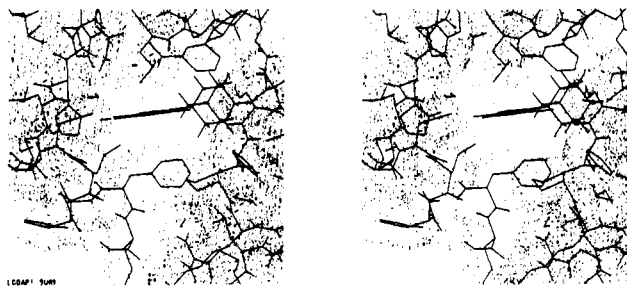


**Figure 7.** Stereoview showing van der Waals surface of *L. casei* DHFR active site with DAPT bound.

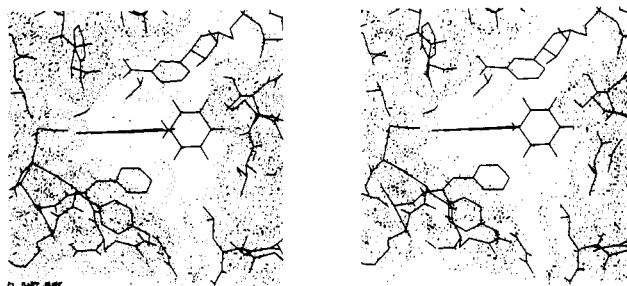


**Figure 8.** Stereoview showing van der Waals surface of chicken liver DHFR active site with DAPT bound.

**Table VI.** Inhibitor Hydrogen-Bonding Patterns for *L. casei* and Chicken Liver DHFR with YETI Modeling Studies

	D...A (Å)		H...A (Å)		<D...H-A (deg)	
	start	after	start	after	start	after
<i>L. casei</i> DHFR						
Asp-26						
O(2)...O(Thr-116)	2.71	2.52	1.75	1.66	175	147
O(2)...N(2)DOPT	2.89	3.19	1.90	2.38	170	137
O(1)...N(3)DOPT	2.64	2.74	1.64	2.53	168	91
O(1)...O(water) <sup>a</sup>	2.57	3.13	1.94	2.37	121	137
DOPT						
O(4)...O(Asp-26)		2.75				
O(4)...O(water)	3.19					
N(2)...O(water)		2.88		1.91		162
N(3)...O(Asp-26)		2.86		2.20		121
Chicken Liver DHFR						
Glu-30						
O(2)...O(Thr-136)	3.36	3.43	2.44	2.50	160	163
O(2)...N(2)DOPT	2.86	2.84	1.86	1.93	174	150
O(1)...N(3)DOPT	2.93	2.67	1.93	2.06	171	116
O(1)...O(water) <sup>a</sup>	2.50	2.74	2.11	1.86	102	151
DOPT						
O(4)...O(water)	2.88	3.26				
O(4)...O(Glu-30)		4.44				

<sup>a</sup> Hydrogen positions are determined by YETI which arbitrarily places those for water. These contact distances are not significant but are only shown for qualitative evaluation of the hydrogen-bonding criteria.

the antifolate orientation, while DOPT was modeled in the folate orientation.

All inhibitor binding models began with a hydrogen-bonding pattern in which the carboxylate oxygens of Asp-26 or Glu-30 were coplanar with N(2) and either N(1) or N(3) of DAMP, DAPT, and DOPT, consistent with the X-ray results of other inhibitor complexes.<sup>8-12</sup> In these enzyme crystal structures there are two structural water molecules which are important to the hydrogen bonding of Asp-26 or Glu-30 and inhibitor. In the *L. casei* structure, both Asp-26 carboxylate oxygen atoms form bifurcated hydrogen bonds, one to the inhibitor and Thr-116 and another to the inhibitor and a structural water molecule. A similar pattern is observed in the chicken liver enzyme structure, although the contact of Glu-30 to Thr-136 is greater than the sum of van der Waals radii. However, in all these models, the bulk of the adamantyl group could not be adequately accommodated as re-

flected by the number of short intermolecular contacts (Tables IV and V), particularly those involving the bacterial enzyme. A comparison of the van der Waals surface of the active site of the bacterial and avian DHFR (Figures 7 and 8) revealed that the inhibitor is less constrained in the avian enzyme.

YETI minimizations of all models relieve the shortest contacts while in general maintaining reasonable hydrogen-bonding patterns with the acidic residue. The only exception is that of DOPT in the bacterial active site (Figure 7). Despite the YETI parameterization preference to maintain hydrogen bond interactions, there is a complete reorientation of the hydrogen bonding of DOPT with Asp-26. Because DOPT occupies a different region of the active site than DAPT (Figure 2), the minimization of DOPT interactions could not simultaneously relieve its adamantyl contacts and maintain the pteridine hydrogen bonding as observed in DAPT (Figure 4).

To relieve the adamantyl short contacts, DOPT is pushed deeper into the active site causing the Asp-26 oxygens to break the O(2)···N(3) and O(1)···N(2) hydrogen bonds of the starting model. As indicated in Table VI, YETI minimization disrupts this hydrogen bonding such that the Asp-26 O(2) is more strongly hydrogen bonded to Thr-116, while the contact to N(2) is significantly weakened. The contacts to Asp-26 O(1) are no longer in hydrogen-bonding distance to its neighbors. However, a new hydrogen bond is formed involving the other N(2) amine hydrogen and a water molecule, previously too far away. The most interesting result of the movements of the Asp-26 side chain and

DOPT is that the Asp-26 backbone keto function, O(26), is now involved in close contacts to N(3) and O(4) of DOPT. Data in Table VI suggest that a hydroxy resonance at O(4) of DOPT would enhance its hydrogen-bonding geometry to O(26).

A similar analysis of chicken liver DHFR (Table VI) reveals that the Glu-30 contacts to Thr-136 are outside hydrogen-bonding contact, and the hydrogen bonds are weaker in general. This is a reflection of the difference in the size of the active site of bacterial and avian DHFR (Figures 7 and 8).

Thus, these YETI modeling studies have shown that the antifolates DAMP and DAPT can be accommodated better in the active site of the avian DHFR than in the bacterial enzyme, in agreement with activity data. In addition, modeling studies with DOPT in the folate orientation show unexpected enzyme interactions in the bacterial enzyme which suggest that it is unlikely to function as a folate in this system.

**Acknowledgment.** The authors thank Drs. Sigmund Zakrzewski and Sue Opitz for providing samples of DAPT. This research was supported in part by research Grants NCI-34714 and FRA-287 (V.C.) from the American Cancer Society Faculty Research Award.

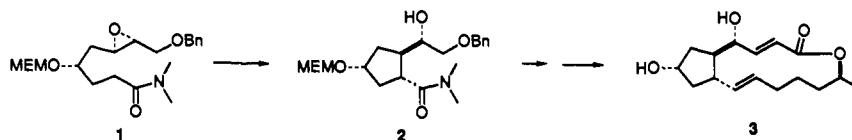
**Supplementary Material Available:** Tables of atomic partial charges, anisotropic thermal parameters, hydrogen atom parameters and geometry (7 pages); table of structure factor amplitudes (50 pages). Ordering information is given on any current masthead page.

## Cyclopentane Construction with Control of Side Chain Configuration: Enantioselective Synthesis of (+)-Brefeldin A

Douglas F. Taber,\* Lee J. Silverberg, and Edward D. Robinson

Contribution from the Department of Chemistry & Biochemistry, University of Delaware, Newark, Delaware 19716. Received March 21, 1991

**Abstract:** Intramolecular opening of an enantiomerically pure epoxide by an amide enolate (**1** → **2**) is shown to be an effective method for cyclopentane construction with control of both ring and side chain absolute configuration. This opening serves as the key step in a synthesis of the Golgi apparatus-blocking macrolide (+)-brefeldin A (**3**). Other features of the synthesis include improved procedures for the enantioselective hydrogenation of a  $\beta$ -keto ester to the corresponding  $\beta$ -hydroxy ester, and for the Julia-Lythgoe reduction of a  $\beta$ -acetoxy sulfone to the trans alkene.



### Introduction

(+)-Brefeldin A (**3**), first isolated in 1958 from *Penicillium decumbens*,<sup>1</sup> has been shown to have both antifungal and antiviral activity.<sup>2</sup> More recently, it has been shown that the antiviral

activity of **3** is due to inhibition by **3** of the intracellular transport of secretory proteins.<sup>3</sup> The finding that brefeldin A **3** specifically blocks the movement of proteins from the endoplasmic reticulum<sup>4</sup> to the Golgi apparatus<sup>4</sup> has made **3** a powerful tool for biochemical investigation.<sup>5</sup>

(1) Singleton, V. L.; Bohonos, N.; Ullstrup, A. J. *Nature* **1958**, *181*, 1072.  
 (2) (a) Betina, V.; Drobnica, L.; Nemeč, P.; Zenanova, M. *J. Antibiot., Ser. A* **1964**, *17*, 93. (b) Betina, V.; Betinova, M.; Kutkova, M. *Arch. Mikrobiol.* **1966**, *55*, 1. (c) Tamura, G.; Ando, K.; Suzuki, S.; Takatsuki, A.; Arina, K. *J. Antibiot.* **1968**, *28*, 160. (d) Takatsuki, A.; Yamaguchi, I.; Tamura, G.; Misato, T.; Arima, K. *J. Antibiot.* **1969**, *22*, 442. (e) Hayashi, T.; Takatsuki, A.; Tamura, G. *J. Antibiot.* **1974**, *27*, 65.

(3) Misumi, Y.; Misumi, Y.; Miki, K.; Takatsuki, A.; Tamura, G.; Ikehara, Y. *J. Biol. Chem.* **1986**, *261*, 11398.

(4) Oda, K.; Hirose, S.; Takami, N.; Misumi, Y.; Takatsuki, A.; Ikehara, Y. *FEBS Lett.* **1987**, *214*, 135.

(5) Nuchtern, J. G.; Bonifacino, J. S.; Biddison, W. E.; Klausner, R. D. *Nature* **1989**, *339*, 223.